

**EXPERIMENTAL VERIFICATION OF
FAST REACTOR SAFETY ANALYSIS CODE SIMMER-III
FOR TRANSIENT BUBBLE BEHAVIOR WITH CONDENSATION**

Koji MORITA*, Tatsuya MATSUMOTO, Kenji FUKUDA

Graduate School of Engineering, Kyushu University

6-10-1 Hakozaki, Fukuoka 812-8581, JAPAN

*: morita@nucl.kyushu-u.ac.jp

Yoshiharu TOBITA, Hidemasa YAMANO, Ikken SATO

Advanced Nuclear System R&D Directorate, Japan Atomic Energy Agency

4002 Narita, O-arai, Ibaraki 311-1393, JAPAN

ABSTRACT

Experimental verification of a reactor safety analysis code, SIMMER-III, was performed for transient behaviors of large-scale bubbles with condensation. The objective of the present study is to verify the code for numerical simulations of relatively short-time-scale multi-phase, multi-component hydraulic problems, among which vaporization and condensation, or simultaneous heat and mass transfer, play an important role. In this study, a series of transient bubble behavior experiments, which are dedicated to condensation phenomena with noncondensable gases, was performed. In the experiments, pressurized mixture of noncondensable gas and steam was discharged as a large-scale single bubble into a cylindrical pool filled with stagnant subcooled water. Concentration of noncondensable gas was taken as an experimental parameter as well as species of noncondensable gas. The characteristics of transient behavior of large-scale bubbles with condensation observed in the experiments were estimated through experimental analyses using SIMMER-III. In the experiments with steam condensation, dispersion of the gas mixture discharged into the liquid pool was accompanied by the vapor condensation at the bubble surface. SIMMER-III simulations suggest that the noncondensable gas has less inhibiting effect on condensation of large-scale bubbles. This is a characteristic different from quasi-steady condensation of small-scale bubbles observed in our previous experiments.

1. INTRODUCTION

A concern with ability to reasonably predict consequences of even the most unlikely accident involving liquid-metal cooled fast reactors (LMFRs) has led to detailed studies of postulated core disruptive accidents (CDAs). This is because mechanistic simulation of an accident sequence during a postulated CDA is realized only by using a comprehensive computational tool that systematically models multi-phase thermal-hydraulic and neutronic phenomena occurring during what are known as the transition and expansion phases of CDA. In this area, a reactor safety analysis code, SIMMER-II, was developed as the first practical tool of its kind [1], and has been used in many experimental and reactor analyses [2]. The code has played a pioneering role especially in advancement of the mechanistic simulation of CDAs, but at the same time extensive worldwide code application revealed many limitations due to the code framework as well as needs for model improvement. To alleviate these limitations and thereby to provide a more reliable tool for the analysis of CDAs, the development of a totally new code, SIMMER-III, has been conducted at the Japan Atomic

Energy Institute (JAEA) in collaboration with the Forschungszentrum Karlsruhe (FZK) in Germany, and the Commissariat à l'Energie Atomique (CEA) which also includes the Institut de Radioprotection et de Sûreté Nucléaire (IRSN) in France [3].

In the present study, a new series of transient bubble behavior experiments was performed to verify the practical applicability of SIMMER-III for relatively short-time-scale multi-phase flows with simultaneous phase transition. In the experiments, a large-scale single bubble of pressurized mixture of noncondensable gas and steam was discharged into a cylindrical pool filled with stagnant subcooled water. In the past several research groups performed experiments to study an expanding high-pressure gas or vapor bubble in a vessel filled with liquid. This is because the injection of a high-pressure gas into a stagnant liquid pool is a characteristic phenomenon during the expansion phase of CDA in LMFRs. Moszynski and Ginsenberg [4] reviewed relevant experiments performed up to 1980. In these experiments, a single- or two-phase fluid (gas or superheated liquid) stored in a pressure vessel was discharged into a liquid pool by rupturing diaphragms, with which the liquid pool was separated from the pressure vessel. A system used in the present experiments is similar in form of a basic apparatus used in these experiments. In the present study, the characteristics of transient behaviors of large-scale bubbles with condensation observed in the experiments were also estimated through experimental analyses using SIMMER-III.

2. OVERVIEW OF SIMMER-III MULTI-PHASE MODELS

SIMMER-III is a two-dimensional, multi-velocity-field, multi-phase, multi-component, Eulerian, fluid-dynamics code coupled with a fuel-pin model and a space- and energy-dependent neutron kinetics model [3]. The fundamental equations of the fluid dynamics are based on a so-called multi-fluid model. The code models five basic LMFR core materials: mixed-oxide fuel, stainless steel, sodium, control (B_4C) and fission gas. A material can exist as different physical states, for example fuel needs to be represented by fabricated pin fuel, liquid fuel, a refrozen crust on structure, solid particles, fuel chunks and fuel vapor, although fission gas exists only in the gaseous state. Thus, material mass distributions are modeled by 30 density components, while the energy distributions are modeled by only 17 energy components since some density components are assigned to the same energy component. The structure field components, which consist of fuel pins and can walls, are immobile. Multi velocity fields are modeled to simulate relative fluid motions adequately, such as fuel/steel separation in a molten core pool and inter-penetration of fuel into sodium.

The overall fluid-dynamics solution algorithm is based on a time-factorization (time-splitting) approach developed for AFDM [5], in which intra-cell interfacial area source terms, momentum exchange functions, and heat and mass transfer are determined separately from inter-cell fluid convection. A semi-implicit procedure is used to solve inter-cell convection on an Eulerian staggered mesh and a higher-order differencing scheme [6] is implemented to improve the resolution of fluid interfaces by minimizing numerical diffusion. A simultaneous solution of all the conservation equations would be complex and inefficient numerically, and hence this solution procedure of separating intra-cell transfers from fluid convection is believed to be the most practical algorithm for complex multi-component systems such as SIMMER-III.

In SIMMER-III, the eight fluid energy components (liquid fuel, steel, sodium; fuel, steel and control particles; fuel chunks and vapor mixture) have 28 binary contact modes, and each fluid component can interact with three kinds of structure surfaces (a fuel pin and left/right can walls). The constitutive models describe intra-cell transfer of mass, momentum and energy at the fluid interfaces. SIMMER-III also has a model for convective interfacial areas to

take better account of highly transient flows [7]. The calculations of intra-cell heat and mass transfer include: structure configuration and heat and mass transfer due to structure breakup, multiple flow regime treatment and interfacial areas with source terms, momentum exchange functions for each flow regime, inter-cell heat transfer due to conduction, melting and freezing, vaporization and condensation, etc.

The phase-transition processes occurring at interfaces are described by employing a heat-transfer limited model [8]. These are nonequilibrium processes because the bulk temperature does not generally satisfy the phase-transition condition when the mass transfer occurs at the interface. When the phase transition is predicted at the vapor/liquid and vapor/solid interfaces, the interface temperatures should be determined so as to take account of the effect of noncondensable gases and multicomponent mixtures on vaporization and condensation. Typically, the condensation rate can be reduced significantly when noncondensable gases are present in the vapor mixture due to a buildup of noncondensable-gas concentration at condensation sites, reducing the condensation saturation temperature below the bulk mixture saturation temperature.

The physical model to represent this effect of noncondensable gases and multicomponent mixtures on vaporization/condensation (V/C) processes is based on a study performed originally for SIMMER-II [1]. The equations for this model were obtained by considering the quasi-steady, stagnant Couette-flow boundary layer, as shown Fig. 1, to relate the mass and energy fluxes to the overall forces driving heat and mass transfer. This classical Couette-flow model has been shown to provide a good engineering model for single-component vapor condensation in the presence of noncondensable gases, thus confirming the adequacy of its theory for incorporation in two-fluid computer codes [9,10,11]. In SIMMER-III, the model extended to multicomponent systems was implemented to predict not only the suppression of condensation by noncondensable gases such as a fission gas, but also the phase-transition rate for a vapor component condensing on the surface of a different material with a new solution algorithm [8,12]. The model characterizes the V/C processes associated with phase transition by employing heat-transfer and mass-diffusion limited models that describe the nonequilibrium phase-transition processes occurring at interfaces and the effects of multicomponent mixture on V/C behaviors. Validity of the model and method employed in the present V/C model was successfully demonstrated by analyzing two series of multicomponent phase-transition experiments [8,13,14].

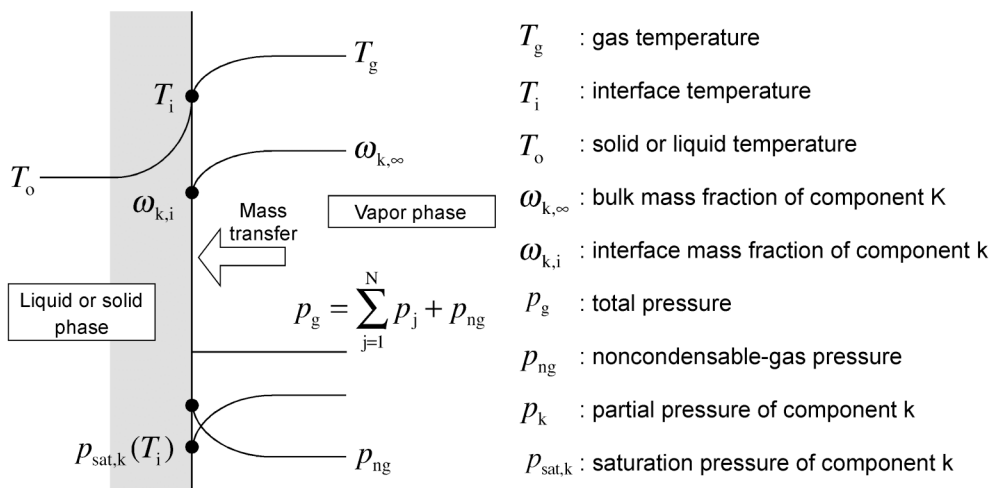


Figure 1 Basis of mass-diffusion limited process
in an N component system with a non-condensable gas.

3. BUBBLE BEHAVIOR EXPERIMENTS

3.1 Experimental procedure

A schematic view of the experimental apparatus and overall arrangement including key dimensions are illustrated in Fig. 2. The basic apparatus consists of a pressure vessel and a cylindrical inner pool (inner diameter 310 mm and height 750 mm), which is surrounded by a larger quadrate outer pool. The confinement vessels of these pools are made of transparent acrylic resin.

The top of the inner water pool was connected to a transparent pipe with an inner diameter of 57 mm. The inner pool was filled with stagnant water at room temperature up to the upper pipe with a height of around 20 ~ 30 cm from the top of the inner pool. In the upper pipe, a floater was set on the water surface as a marker of the water level, from which displacement determines the transient gas volume in the inner pool and the pressure vessel. The outer pool was also filled with water to improve visual observation inside the cylindrical inner pool by minimizing optical distortion, which is caused by the difference in refractive indexes between water and acrylic resin.

The pressure vessel made of stainless steel was connected to the bottom of the inner pool through the adiabatic region. The exits of the adiabatic region and the pressure vessel were initially closed with upper and lower rupture disks, respectively. In the pressure vessel, whose effective capacity was about 600 cm³, a mixture of steam and noncondensable gas was generated and pressurized by boiling water of 8.0 cm³ using an electric heater. The adiabatic region giving an approximate volume of 150 cm³ was initially evacuated down to several kPa by a vacuum pump. This can reduce the heat transfer from the pressure vessel to the inner pool during the pressurization of gas mixture.

Two pressure sensors were installed to measure the pressure transients in the pressure vessel and at the top of the water pool. After the two rupture disks break, the gas mixture was discharged from the pressure vessel into the water pool, expanding in the inner pool. Two high-speed cameras, both of which can record 400 frames per second, were used to record the movements of the gas phase in the inner pool and the water surface level changes in the upper pipe, respectively, as digital motion pictures. Initial temperatures were measured in the inner water pool, the adiabatic region, and the pressure vessel.

Two rupture disks used to seal the pressure vessel and the adiabatic region at the beginning of the experiment were hand-made diaphragms of polyester film. The lower disk was designed to rupture at a desired pressure, while the upper disk, which is thinner than the upper one, has strength enough to stand water head. The break of the lower rupture disk was triggered when the pressure in the pressure vessel reaches the rupture limit of the diaphragm during the pressurization of the gas mixture by electric heating. After the lower rupture disk breaks, the initially pressurized gas mixture spouts into the adiabatic region. The upper rupture disk also breaks subsequently and then the gas mixture starts expanding inside the water pool. The laser detector at the bottom of the inner pool determines the instance of the gas-mixture release into the inner water pool, triggering the two high-speed cameras to begin operating.

Main initial conditions of the experiments are shown in Table 1. Concentration of noncondensable gas in the mixture was taken as an experimental parameter as well as species of noncondensable gas. In the present experiments, nitrogen and xenon were used as a noncondensable gas mixed with steam because of difference in a mass-transfer resistance for the diffusion of steam. The experiments except for the case only using nitrogen gas were performed with similar rupture pressures of about 0.3 MPa. The water subcooling in the inner pool was in the range of around 110 ~ 120 K. In the pressure vessel, the initial gas mixture with water boiling had a very high void fraction, which could suppress two-phase flashing during the gas expansion process.

Table 1 Initial conditions of transient bubble behavior experiments.

	Noncondensable gas mixed with steam					
	Nitrogen			Xenon		
Noncondensable gas concentration (mol%)	0.4	10.3	19.5	100	11.7	20.8
Pressure in pressure vessel (MPa)	0.274	0.287	0.294	0.227	0.287	0.298
Steam saturation temperature (K)	404	402	399	---	401	399
Void fraction in pressure vessel (%)	98.8	98.8	98.7	100	98.7	98.7
Pressure in adiabatic region (kPa)	4.8	4.3	2.5	3.7	2.7	6.1
Water pool temperature (subcooling) (K)	288 (116)	291 (111)	290 (109)	288 ---	284 (117)	289 (110)
Water level in upper pipe (cm)	32.9	24.1	21.9	22.6	27.4	29.6

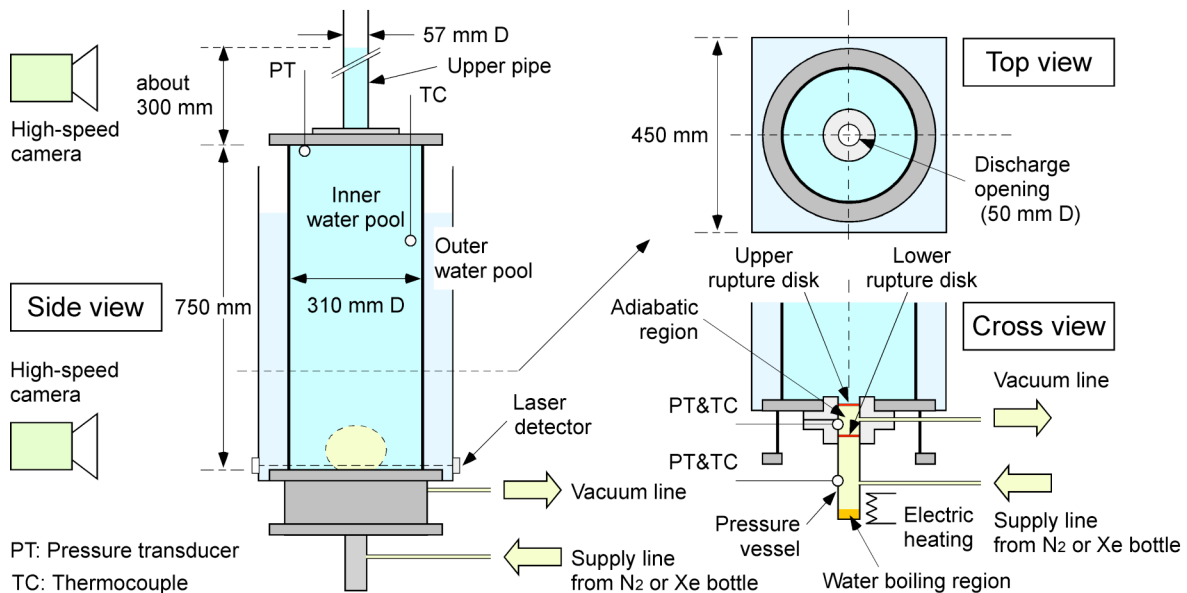


Figure 2 Schematic view of experimental apparatus.

3.2 Experimental results

Gas volume changes defined here correspond to the differences between the instantaneous gas volumes in the experimental processes and the initial gas volumes at the beginning of the experiments. Experimental data for the total gas volume changes in both the water pool and the pressure vessel were obtained from the water level changes in the upper pipe of the experimental setup.

Figure 3 shows the experimental results of the gas volume changes of the four cases, in which different nitrogen-gas concentrations were used. Here, the time zero is defined by the triggering of the lower diaphragm rupture. The results of all cases show that once the lower and upper rupture disks break, the gas volume begins to increase with the expansion of the originally pressurized gas in the pressure vessel, while not more than a hundred millisecond

the gas volume starts to decrease. This occurs because, as the gas expands, the pressure of the gas becomes lower than the atmospheric pressure due to the steam condensation and/or the inertia of the water slug moving upward. When the gas pressure decreases to a value that is smaller than the surrounding pressure, the gas will be compressed, and as a result its volume decreases.

By comparing the experimental results between the four cases shown in Fig. 3 it can be seen that when the nitrogen-gas concentration is larger, the corresponding gas volume change, especially the maximum gas volume change, is much larger. The experimental results also show that the larger the nitrogen-gas concentration, the longer the period of the gas expansion.

The effect of thermophysical properties of noncondensable gas on condensation was also investigated by comparison between steam-nitrogen and steam-xenon systems. Figure 4 indicates the experimental results of the gas volume changes in the cases using the noncondensable gas of around 10 and 20 mol%. As shown in Fig. 4 the expansion period of the gas in the steam-xenon system becomes longer than that in the steam-nitrogen system under a similar concentration of noncondensable gas although the maximum gas volume change in the steam-xenon system is comparable to that in the steam-nitrogen. This might be because a mass-transfer resistance for the diffusion of steam toward the condensation interface in the steam-xenon system is larger than that in the steam-nitrogen one due to the larger molecular weight of xenon than that of nitrogen.

In Figs. 5 and 6, images of the gas phase in the water pool are shown for the cases using a different initial concentration of noncondensable gas at selected time intervals. In these figures, the time zero is defined by the instance when the gas mixture is released into the water pool. The experimental images obtained using a high-speed camera represent a 180 mm (width) \times 150 mm (height) region, of which base corresponds to the bottom of the water pool. As can be seen from Fig. 5, in the case using steam mixed with a very small amount of nitrogen gas the gas mixture discharged into the water pool disperses like bubbly flows due to rapid condensation, and forms no large-scale bubble as observed in the case using only nitrogen gas. In the cases using mixture of nitrogen gas and steam, Fig. 6 also indicate the similar behavior around the bubble surface, where dispersive mixing of the gas and liquid phases is observed.

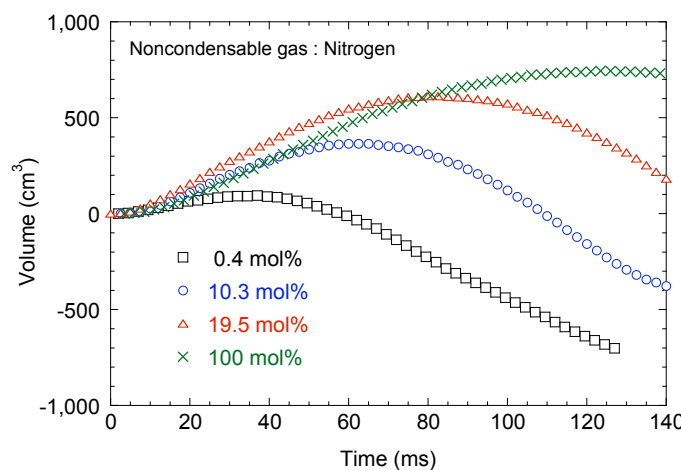


Figure 3 Comparison of gas volume change between experimental cases using a different concentration of nitrogen gas.

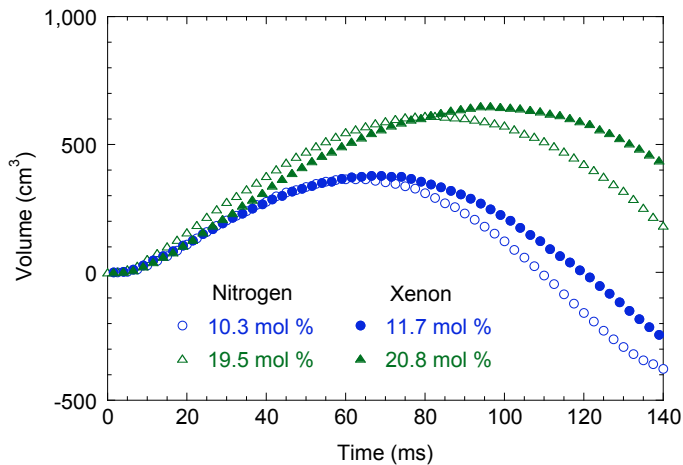


Figure 4 Comparison of gas volume change between experimental cases using nitrogen and xenon as a noncondensable gas.

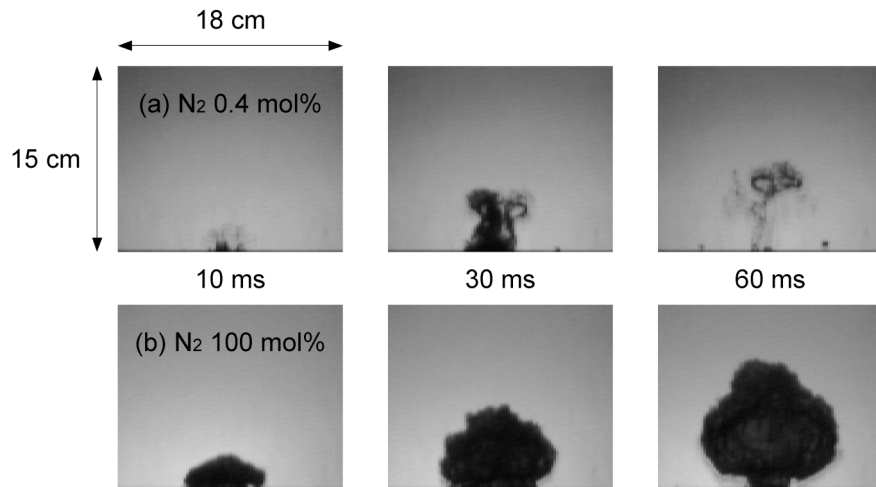


Figure 5 Comparison of bubble shape change in water pool between experimental cases using almost only steam and only nitrogen gas.

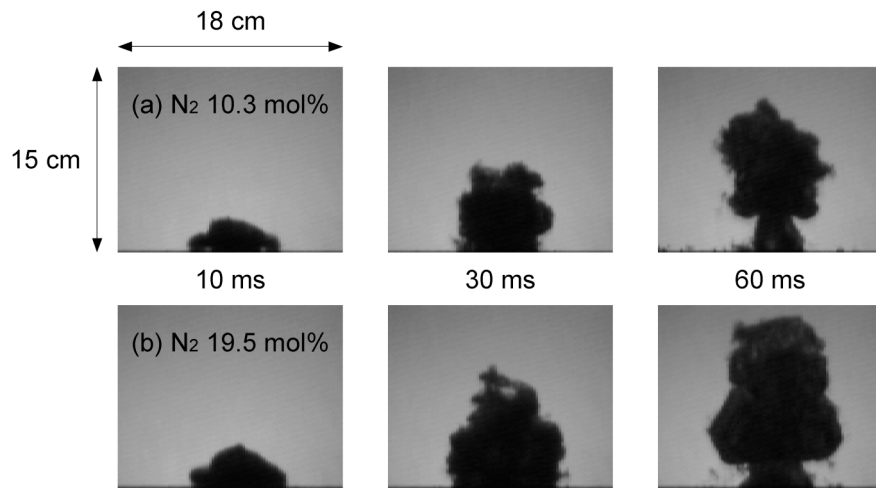


Figure 6 Comparison of bubble shape change in water pool between experimental cases using a different concentration of nitrogen gas.

4. EXPERIMENTAL ANALYSES

4.1 Reference calculation

Figure 7 shows a schematic view of the analytical geometry used in the SIMMER-III calculations for the corresponding experimental setup shown in Fig. 2. In the calculations, five regions of the pressure vessel, the adiabatic region, the inner water pool, the upper pipe and the atmosphere were modeled to represent experimental conditions by a two-dimensional cylindrical geometry. For the water pool region, 18 radial and 75 axial computational cells were used. Simulation results of the gas volume change and the pressure change in the pressure vessel as the reference case using only nitrogen gas are indicated in Figs. 8 and 9, respectively, in comparison with the corresponding experimental results. SIMMER-III well reproduces the experimental results of the transient behavior of bubble expansion.

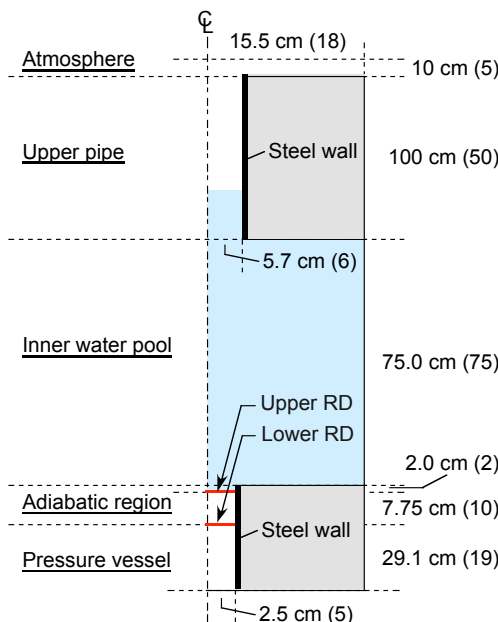


Figure 7 SIMMER-III geometry for analyses of experiments with bubble condensation (the number in parentheses is the number of the computational mesh cells).

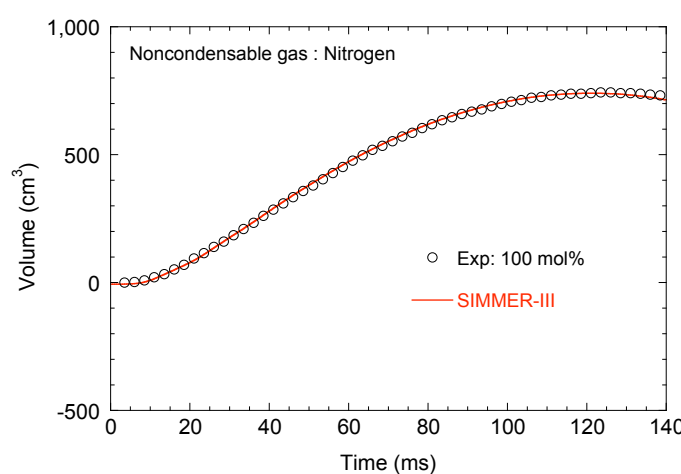


Figure 8 Simulation results of gas volume change for the reference case using only nitrogen gas.

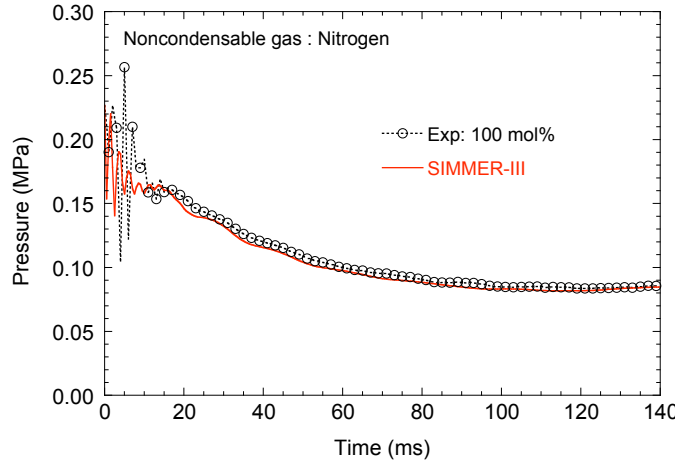


Figure 9 Simulation results of pressure change in the pressure vessel for the reference case using only nitrogen gas.

4.2 Effect of noncondensable gas on condensation

In the present system, during discharge of the gas mixture from the pressure vessel to the water pool, steam condensation can occur mainly on both the cold structure surface of the adiabatic region and the bubble surface in the subcooled water pool. Therefore, the present numerical simulations using SIMMER-III were performed to investigate the inhibiting effect of noncondensable gas on condensation at the gas/solid (G/S) and gas/liquid (G/L) interfaces.

Figures 10 and 11 show the simulation results of the gas volume change and the pressure change in the pressure vessel in the case using nitrogen gas of 19.5 mol%, respectively, in comparison with the corresponding experimental results. In these figures, three parametric results of the simulations are presented. The first two cases consider the nitrogen-gas effect on condensation at the G/S and G/L interfaces and at the G/S interface, respectively. The third considers no nitrogen-gas effect on condensation at any interface. As can be seen from these figures, SIMMER-III simulations considering the nitrogen-gas effect on condensation only at the G/S interface fairly well reproduce the experimental results represented by the gas volume change and the pressure change in the pressure vessel. The results of the gas volume change in the cases using nitrogen gas of 10.3 and 0.4 mol% are indicated in Figs. 12 and 13, respectively. Good agreements with the experimental results were also obtained in the simulations considering the nitrogen-gas effect only at the G/S interface.

It can be seen from the comparisons of the above simulation results that much more condensation occurs at the G/L interface rather than at the G/S interface as the nitrogen-gas concentration increases. The present results suggest that under the present experimental conditions the nitrogen gas has less effect on steam condensation at the G/L interface, while the condensation at the G/S interface is reduced due to a buildup of nitrogen gas at which condensation occurs.

Figure 14 shows the comparison of the simulation results in the cases using xenon gas of 11.7 and 20.8 mol%. The simulations considering the xenon-gas effect only at the G/S interface result in fairly better agreement with the experimental results. It seems that SIMMER-III also represents the effect of thermophysical properties of noncondensable gas on steam condensation at the G/S interface reasonably.

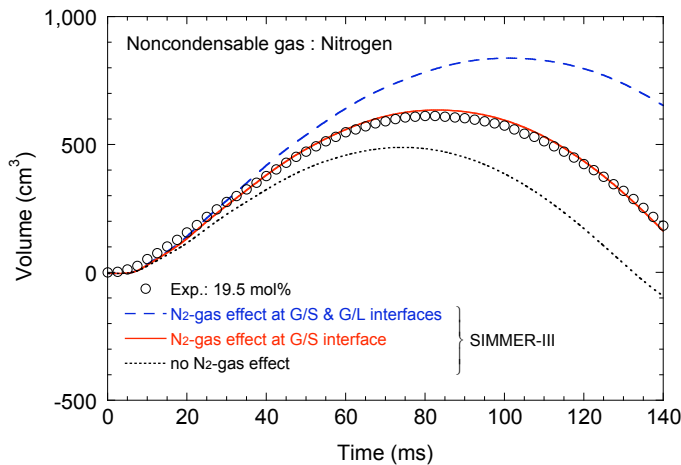


Figure 10 Effect of nitrogen gas at G/S and G/L interfaces on gas volume change (nitrogen-gas concentration of 19.5 mol%).

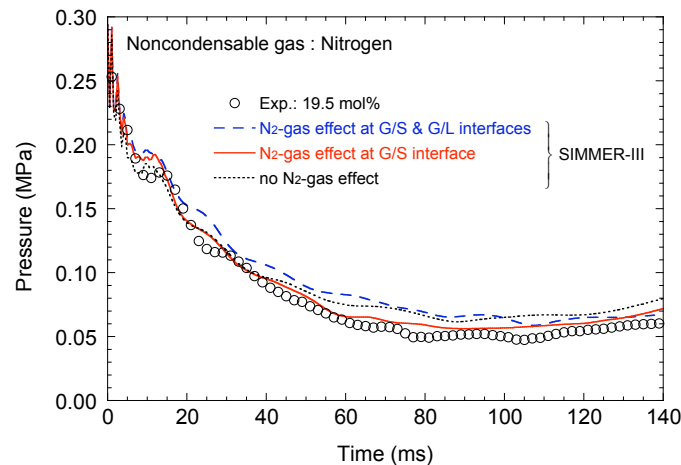


Figure 11 Effect of nitrogen gas at G/S and G/L interfaces on pressure change in the pressure vessel (nitrogen-gas concentration of 19.5 mol%).

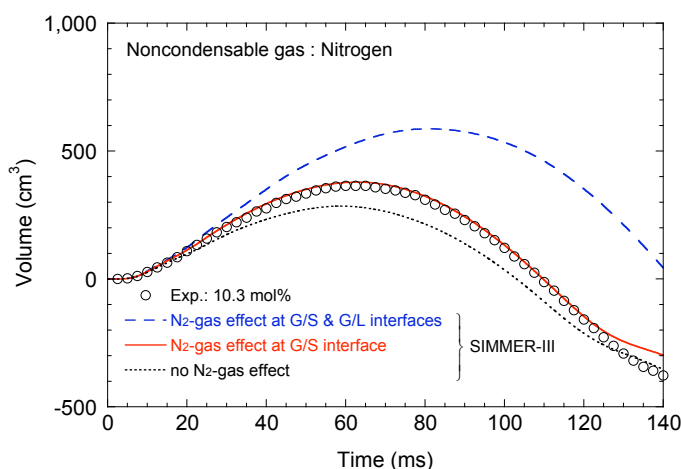


Figure 12 Effect of nitrogen gas at G/S and G/L interfaces on gas volume change (nitrogen-gas concentration of 10.3 mol%).

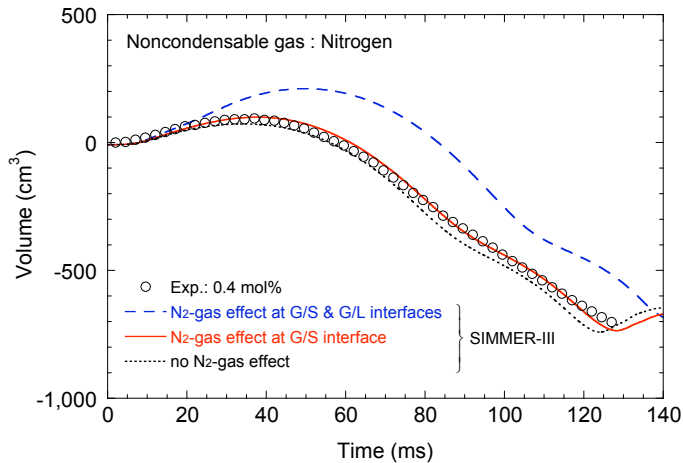


Figure 13 Effect of nitrogen gas at G/S and G/L interfaces on pressure change in the pressure vessel (nitrogen-gas concentration of 0.4 mol%).

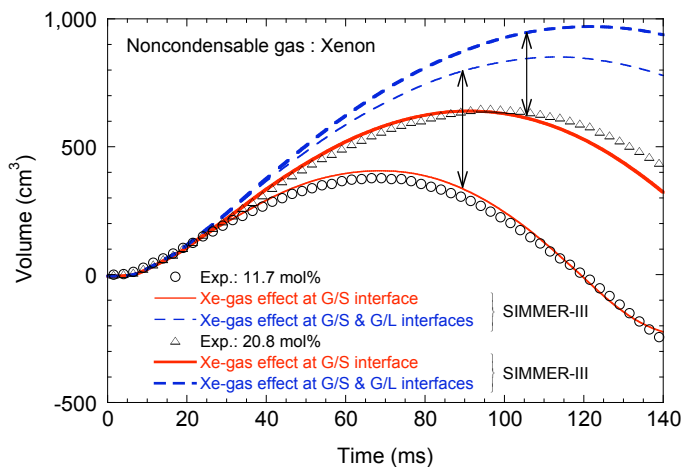


Figure 14 Effect of xenon gas on condensations at G/L interface (xenon-gas concentrations of 11.7 and 20.8 mol%).

4.3 Discussion

The present numerical simulations suggest that there is less inhibiting effect of noncondensable gas on vapor condensation of large-scale bubbles discharged into a stagnant subcooled liquid. This is a characteristic different from quasi-steady condensation of small-scale bubbles observed in our previous experiments [13,14], where the condensation rate was reduced dominantly by noncondensable gas mixed with steam. In the present experiments with steam condensation, as can be seen from Figs. 5 and 6, dispersion of the gas mixture discharged into the liquid pool was accompanied by the steam condensation at the bubble surface. This might be relevant to one of the liquid entrainment mechanisms in the bubble expansion process, the condensation-induced instability or condensation shock [4,15]. Such dynamic mixing of the gas and liquid phases induced by condensation would prevent a buildup of the noncondensable gas on the bubble surface. This results in the less inhibiting effect of the noncondensable gas on condensation. The comparison with our previous experiments using small-scale bubbles [13,14] suggests that the characteristics observed in

large-scale bubble condensation disappear in condensation of small-scale bubbles, where local two-phase mixing might not develop around their surface.

5. CONCLUSION

A series of experiments was performed for transient behaviors of large-scale bubble with condensation. Characteristics of the bubble behaviors observed in the experiments were estimated through the experimental analyses using the reactor safety analysis code SIMMER-III. SIMMER-III simulations suggest that the noncondensable gas has less inhibiting effect on condensation of large-scale bubbles, in which the gas and liquid phases are dispersively mixed without a buildup of the noncondensable gas. The present study indicates that SIMMER-III can simulate the condensation processes of large-scale bubbles under the effect of noncondensable gas reasonably in sufficient physical details. We expect that the present results will contribute to the improvement of reliability in accident analyses of LMRs.

ACKNOWLEDGEMENTS

This work was performed as a joint research between JAEA and Kyushu University. The authors wish to thank Shin-ichi Tanoue and Hiromasa Yanagisawa of Kyushu University for their contributions to this work.

REFERENCES

- [1] W.R. BOHL, L.B. LUCK, SIMMER-II: A Computer Program for LMFR Disrupted Core Analysis, LA-11415-MS, Los Alamos National Laboratory (1990).
- [2] L.L. SMITH, C.R. BELL, W.R. BOHL, L.B. LUCK, T.R. WEHNER, G.P. DEVAULT, F.R. PARKER, The SIMMER Program: Its Accomplishment, *Proc. Int. Mtg. on Fast Reactor Safety*, 977, Knoxville, TN, April 1985 (1985).
- [3] Y. TOBITA, S. KONDO, H. YAMANO, S. FUJITA, K. MORITA, W. MASCHEK, P. COSTE, S. PIGNY, J. LOUVET, T. CADIOU, "The development of SIMMER-III, an advanced computer program for LMFR safety analysis," *Proc. Joint IAEA/NEA Technical Meeting on the Use of Computational Fluid Dynamics Codes for Safety Analysis of Reactor Systems (including Containment)*, Pisa, Italy, Nov. 11-13, 2002 (2002).
- [4] J.R. MOSZYNNSKI, T. GINSBERG, Liquid Entrainment by an Expanding Gas or Vapor Bubble – A Review of Experiments and Models, BNL-NUREG-2B343, Brookhaven National Laboratory (1980).
- [5] W.R. BOHL, D. WILHELM, F.R. PARKER, J. BERTHIER, L. GOUTAGNY, H. NINOKATA, AFDM: An Advanced Fluid-Dynamics Model, Volume I: Scope, approach, and summary, LA-11692-MS, Vol. I, Los Alamos National Laboratory (1990).
- [6] B. VAN LEER, "Towards the ultimate conservative difference scheme. IV. a new approach to numerical convection," *J. Compt. Phys.*, **23**, 276 (1977).
- [7] Y. TOBITA, K. MORITA, S. KONDO, N. SHIRAKAWA, W.R. BOHL, F.R. PARKER, D.J. BREAR, "Interfacial area modeling for a multi-phase, multi-component fluid-dynamics code," *Proc. Int. Conf. on Multi-phase Flows '91-TSUKUBA*, **2**, 361, Tsukuba, Japan, Sept. 24-27, 1991 (1991).

- [8] K. MORITA, T. MATSUMOTO, R. AKASAKA, K. FUKUDA, T. SUZUKI, Y. TOBITA, H. YAMANO, S. KONDO, "Development of multicomponent vaporization/condensation model for a reactor safety analysis code SIMMER-III: theoretical modeling and basic verification," *Nucl. Eng. Des.*, **220**, 224 (2003).
- [9] S.M. GHIAASIAAN, B.K. KAMBOJ, S.I. ABDEL-KHALIK, "Two-fluid modeling of condensation in the presence of noncondensables in two-phase channel flows," *Nucl. Sci. Eng.*, **119**, 1 (1995).
- [10] G.F. YAO, S.M. GHIAASIAAN, D.A. EGHBALI, "Semi-implicit modeling of condensation in the presence of non-condensables in the RELAP5/MOD3 computer code," *Nucl. Eng. and Des.*, **166**, 217 (1996).
- [11] G.F. YAO, S.M. GHIAASIAAN, "Numerical modeling of condensing two-phase flows," *Numerical Heat Transf., B*, **30**, 137 (1996).
- [12] K. MORITA, T. MATSUMOTO, R. AKASAKA, K. FUKUDA, T. SUZUKI, Y. TOBITA, H. YAMANO, S. KONDO, "Advanced modeling of multicomponent vaporization/condensation phenomena for a reactor safety analysis code SIMMER-III," *Proc. 10th Int. Conf. on Nuclear Engineering*, ICONE10-22229, Arlington, VA, April 2002 (2002).
- [13] T. SUZUKI, Y. TOBITA, H. YAMANO, S. KONDO, K. MORITA, T. MATSUMOTO, R. AKASAKA, K. FUKUDA, "Development of multicomponent vaporization/condensation model for a reactor safety analysis code SIMMER-III: extended verification using multi-bubble condensation experiment," *Nucl. Eng. Des.*, **220**, 240 (2003).
- [14] K. MORITA, K. FUKUDA, Y. TOBITA, S. KONDO, T. SUZUKI, W. MASCHEK, "Generalized modeling of multi-component vaporization/condensation phenomena for multi-phase-flow analysis," *Proc. German-Japanese workshop on multi-phase flow*, Karlsruhe, Germany, Aug. 26-28, 2002, FZKA 6759, Forschungszentrum Karlsruhe (2003).
- [15] D.J. SIMPSON, M. SAITO, T.G. THEOFANOUS, "The termination phase of core disruptive accidents in LMFBR," PNE-81-151, Purdue University (1980).